Arch. Metall. Mater. **68** (2023), 3, 881-886

DOI: https://doi.org/10.24425/amm.2023.145451

LONG CHEN[1,2*]

MICROSTRUCTURE EVOLUTION, PHASE COMPOSITION, TENSILE AND HARDNESS PROPERTIES INVESTIGATION OF $CrCuFeNi_2TI_X$-BASED HIGH-ENTROPY ALLOYS

$CrCuFeNi_2Ti_x$ high-entropy alloys (HEAs) (x = 0.1 ~ 0.7) are prepared and studied in this paper to investigate the effect of titanium on the microstructure, phase composition, and mechanical properties of the $CrCuFeNi_2Ti_x$-based system. Microstructural studies using scanning electron microscopy (SEM) and X-ray diffraction (XRD) showed that the addition of titanium could induce the formation of a body-centered cubic lattice (BCC) and intermetallic compounds (Ni_3Ti) of the $CrCuFeNi_2Ti_x$-based system. The practical formation of the phases meet the theory of the atomic size difference δ, mixing enthalpy ΔH_{mix}, mixing entropy ΔS_{mix}, valence electron concentration (*VEC*), and electronegativity difference $\Delta\chi$. Additionally, the tensile and hardness properties of the $CrCuFeNi_2Ti_x$-based system are investigated in this study. Generally, $CrCuFeNi_2Ti_x$ HEAs show low stiffness and good flexibility in mechanical properties. When the x value is relatively small, the HEAs show good ductility in the tensile test, which is the result of a face-centered cubic lattice (FCC) in the phase composition at this stage; when the x value becomes larger, due to the formation of the intermetallic compounds Ni_3Ti, the HEAs show high hardness.

Keywords: high entropy alloys; phase composition; microstructure; tensile tests; hardness test

1. Introduction

In 1995, the traditional alloy design was broke through with a large number of experiments by Yeh et al. and his group from Taiwan. He proposed this new material design concept, high entropy alloy (HEA), which contains five or more kinds of metal elements but tend to form face-centered cubic lattice (FCC) and body-centered cubic lattice (BCC) crystal structures [1,2]. The FCC and BCC crystal structures could provide unique mechanical properties, for example, high hardness [3-5], high temperature softening resistance [6-10], high strength [8,9,11], and high wear resistance [12,13]. In recent decades, HEA is called one of the three biggest breakthrough in the alloy's research field [14,15].

Mainly, the phase composition of the solid solutions in HEAs is responsible for their unique mechanical properties. It has been proposed by Zhang et al. that the important factors for the formation of solid solutions in HEAs are the atomic size difference δ, mixing enthalpy ΔH_{mix}, and mixing entropy ΔS_{mix} [16,17]. In particular, if a solid solution could be formed in HEAs, δ should be less than 8.5%, ΔH_{mix} should be –22 kJ/mol to 7 kJ/mol, and ΔS_{mix} should be 11 J/(K·mol) to 19.5 J/(K·mol) [18]. To explain the formation of solid solution and amorphous phase in HEAs further, the valence electron concentration (*VEC*) and electronegativity difference $\Delta\chi$ theories were reported by Guo et al. and Fang et al. [18-20]. In their studies, $\Delta\chi$ is defined as an important parameter in the formation of bulk metallic glasses (BMG), while VEC can be used to quantitatively predict the phase stability for FCC and BCC phases. Particularly, sole FCC phase exists when $VEC > 8$, mixed FCC and BCC phases will co-exist when $6.87 < VEC < 8$, and sole BCC phase exists when $VEC < 6.87$.

In this paper, the aforesaid phase prediction theories are verified by scanning electron microscopy (SEM) and X-ray diffraction (XRD) test of casted $CrCuFeNi_2Ti_x$ HEAs ($x = 0.1 \sim 0.7$). Based on the *VEC* scheme, a series of $Al_{0.5}CoCrCuFeNi$ and $Al_{0.5}CrCuFeNi_2$ HEAs were developed in the previous studies [21,22]. It was shown that these series of as-cast HEAs with disordered FCC structures and a dendritic morphology showed sufficient tensile plasticity. Moreover, it was confirmed that for the $Ti_xCoCrFeNiCu_{1-y}Al_y$ HEAs, after adding Ti element, the phase composition will change from FCC to BCC + intermetallic compounds [23]. The content of Ti in HEAs will be the key to determine the microstructure and mechanical properties, and it is worth for a further research. On that basis, we developed the

[1] NORTHWESTERN POLYTECHNICAL UNIVERSITY, THE SCHOOL OF MECHANICAL ENGINEERING, XI'AN, CHINA
[2] SHENZHEN UNIVERSITY, COLLEGE OF ELECTRONICS AND INFORMATION ENGINEERING, SHENZHEN, CHINA

* Corresponding author: chenmf767@foxmail.com

target $CrCuFeNi_2Ti_x$ HEAs used in this extensively work, but fully replaced the Al element with Ti.

In what follows, Section 2 describes the experimental procedure in this research. Section 3 shows the corresponding experimental study results and discussions. At last, the main conclusions are described in Section 4.

2. Experimental procedure

To prepare for subsequent SEM, XRD, tensile and hardness test, slabby and cylindrical ingots of the $CrCuFeNi_2Ti_x$ HEAs were produced by a 50 g capacity high vacuum arc-melting and casting furnace, respectively. The purities of all the metal element samples are beyond 99.999% wt.%, and all the samples were weighed by an electronic balance with sensitivity equal to 0.0001 g. Argon gas was used as a protective gas during melting and casting, while the air pressure was exhausted under 1×10^{-4} by mechanical, electromagnetic and molecular pump at the beginning. Pure Ti metal was melted three times before casting to deplete the residual oxygen, and all the alloys were at least re-melted three times before casting into ingots in order to obtain homogeneity. The alloys were cooled down for 20 minutes before being taken out. The crystal structures of the $CrCuFeNi_2Ti_x$ HEAs were identified by XRD by using SmartLab XRD with Cu-Kα radiation. For all the samples, the same experimental settings of the XRD were adopted to enable the direct comparison of diffraction intensities. The voltage and current were 45 kV and 200 mA, respectively. The scanning resolution was 5 deg/min with 0.02 deg/step from 30 deg to 130 deg. Hardness test specimens of the $CrCuFeNi_2Ti_x$ HEAs were wire-cut into cylinders with a thickness of 3 mm, and the surface was polished by grit size 320, 800, 1200 and 2000 abrasive paper, and micro 1 and 0.3 alumina suspension. The hardness of the specimens was measured by using a micro hardness tester (Future-Tech Corp.) under a test load of 1000 gf for 15 s. And the microstructures of hardness test specimens were examined by using a microscope (Nikon Model Epiphot 200). For every hardness test specimen, measurements were performed ten times. The tension specimens of the $CrCuFeNi_2Ti_x$ HEAs were wire-cut into a length of 58 mm, with a width of 13.2 mm. The illustration and a snapshot of the specimens are show in the Fig. 1 below. In Fig. 1(b) wrinkles appeared after the tensile test of $CrCuFeNi_2Ti_{0.1}$. All the specimens were ground and polished to a thickness around 1 mm in order to avoid the casting defect. The tensile tests were carried out at room temperature (RT) with MTS Alliance RT/50 testing machine operating at a strain rate of 1×10^{-3} s^{-1}. For one particular x value, six samples were prepared. At last, the microstructures of the fragments of tensile specimens were examined by using a SEM (Oxford-7573).

3. Results and discussion

3.1. Phase Composition

As noted in introduction section, ΔH_{mix}, ΔS_{mix}, δ, VEC, and $\Delta\chi$ play important roles in determining the HEA phase composition. The mixing enthalpy ΔH_{mix} could be expressed as

$$\Delta H_{mix} = \sum_{i=1,\, i\neq j}^{N} \Omega_{ij} c_i c_j \tag{1}$$

in which $\Omega = 4\Delta H_{AB}^{mix}$ is the regular melt-interaction parameter between the i^{th} and j^{th} elements, ΔH_{AB}^{mix} is the mixing enthalpy of binary liquid AB alloys, and N is the total number of elements involved. The variables c_i and c_j are the composition of the i^{th} element and j^{th} element, respectively [26,27]. The mixing entropy ΔS_{mix} could be expressed as

$$\Delta S_{mix} = -R\sum_{i=1}^{N} c_i \ln c_i \tag{2}$$

in which R is the gas constant [28,29]. The atomic size difference δ could be expressed as

$$\delta = \sqrt{\sum_{i=1}^{N} c_i \left(1 - r_i/\bar{r}\right)^2} \tag{3}$$

in which r_i is the atomic radius of the i^{th} element and $\bar{r}$ is the average atomic radius. The electronegativity difference $\Delta\chi$ could be defined by

$$\Delta\chi = \sqrt{\sum_{i=1}^{N} c_i \left(\chi_i - \bar{\chi}\right)^2} \tag{4}$$

in which χ_i is the i^{th} element's Pauling electronegativity and $\bar{\chi}$ is the average Pauling electronegativity [19]. The VEC could be defined by

$$VEC = \sum_{i=1}^{N} c_i \left(VEC\right)_i \tag{5}$$

in which $(VEC)_i$ is the VEC for the individual elements.

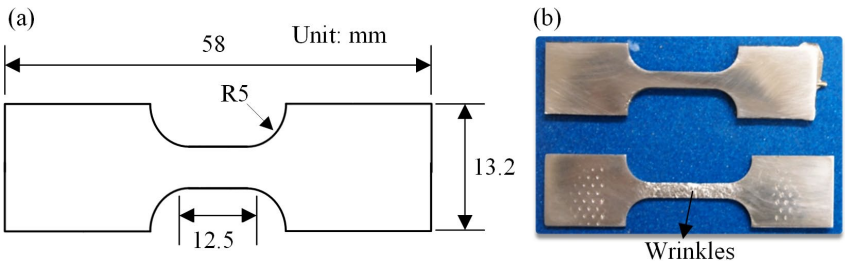

Fig. 1. Illustration (a) and snapshot (b) of the $CrCuFeNi_2Ti_{0.1}$ specimen

All these five parameters were calculated for $CrCuFeNi_2Ti_x$ HEAs and listed in Table 1. Clearly, The ΔH_{mix} values are between –22 kJ/mol and 7 kJ/mol, while δ values are less than 8.5%, and ΔS_{mix} values are between 11 J/(K·mol) and 19.5 J/(K·mol). As these three phase prediction criteria addressed, the solid solution could successfully form in $CrCuFeNi_2Ti_x$ HEAs. Moreover, according to the calculated VEC and $\Delta\chi$ values, the formation of the FCC phase was favored in $CrCuFeNi_2Ti_x$ HEAs.

TABLE 1

Parameters of ΔH_{mix}, ΔS_{mix}, δ, *VEC*, and $\Delta\chi$ for $CrCuFeNi_2Ti_x$

Alloy	ΔH_{mix} (kJ/mol)	ΔS_{mix} J/(K·mol)	δ (%)	*VEC*	$\Delta\chi$
$CrCuFeNi_2Ti_{0.1}$	0.569	13.552	3.9	8.90	0.104
$CrCuFeNi_2Ti_{0.2}$	–0.976	13.718	4.3	8.81	0.110
$CrCuFeNi_2Ti_{0.3}$	–2.407	13.884	4.6	8.72	0.116
$CrCuFeNi_2Ti_{0.4}$	–3.731	14.051	4.9	8.63	0.121
$CrCuFeNi_2Ti_{0.5}$	–4.959	14.134	5.1	8.55	0.126
$CrCuFeNi_2Ti_{0.7}$	–7.15	14.513	5.6	8.39	0.134

However, as it is presented in Fig. 2, although the FCC phases are the dominating phase in the $CrCuFeNi_2Ti_x$ system, the BCC structure and intermetallic compounds (Ni_3Ti) show up when the *VEC* value becomes smaller, ΔX gets close to 0.133, and $x = 0.7$. It is worth noting that although the hardness of HEAs will increase due to the formation of Ni_3Ti, both the plasticity and the yield strength will decrease dramatically. Since the intermetallic compound phases are unstable, particular notice should be taken in the following test of mechanical properties.

3.2. Tensile behavior and fracture surface

Compared to compression tests, fewer tensile tests of HEAs have been reported in the past, especially at room temperature. The main reason for this is the apparent contradiction between high strength and high tensile ductility for alloys. Generally, the FCC structured alloys usually have good tensile ductility and

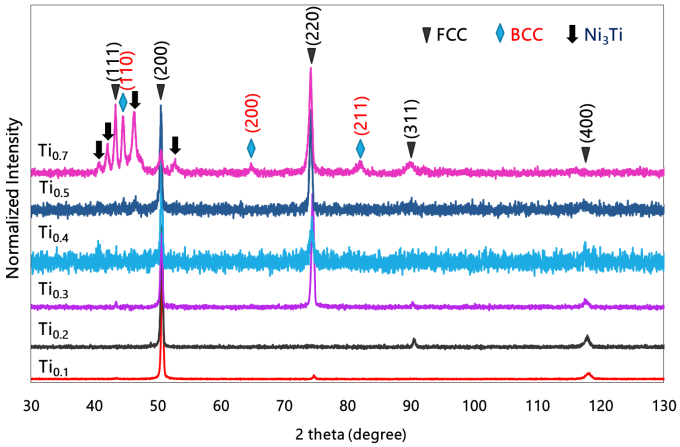

Fig. 2. XRD patterns of the as-cast $CrCuFeNi_2Ti_x$ (x = 0.1, 0.2, 0.3, 0.4, 0.5 and 0.7)

low strength, while the BCC phase containing alloys have high strength and poor tensile ductility [24]. In this paper, we measured the tensile properties of as-cast solely FCC structured and FCC + BCC + intermetallic compound phase containing HEAs to explore the existence of the confluence of high strength and high tensile ductility for HEAs.

Representative engineering stress-strain curves for the as-cast $CrCuFeNi_2Ti_x$ (x = 0.1, 0.3, 0.5 and 0.7) HEAs are presented in Fig. 3, and the statistical results of the yield strength, ultimate tensile strength (UTS), and Young's modulus are given in Fig. 4. Furthermore, the corresponding fracture surface morphologies are shown in Fig. 5. Clearly the $CrCuFeNi_2Ti_{0.1}$ HEAs have good ductility as it is shown. As the content of Ti increases, the scatterings on the yield strength and fracture strength were reasonable, while the variation in tensile elongation was large. The as-cast $CrCuFeNi_2Ti_{0.1}$ with disordered FCC structures has, on average, a yield stress of 236.4 (±42.1) MPa, a UTS of 458.3 (±39.8) MPa and a Young's modulus of 47.3 (±3.9) GPa. The fractured surfaces in Fig. 5 (a) and (b) show a dimple-like morphology, which is a typical ductile deformation behavior. The UTS reaches maximum (954.9 (±86.2) MPa) when x = 0.5, and the yield stress reaches maximum (573.6 (±43.7) MPa) when x = 0.7.

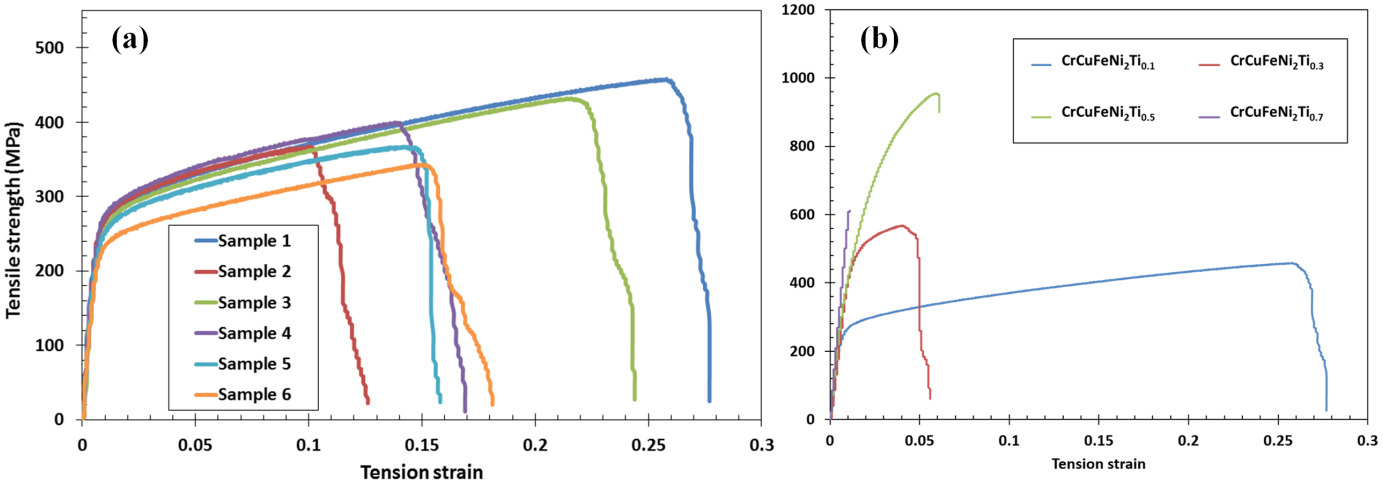

Fig. 3. Tensile behavior of (a) the $CrCuFeNi_2Ti_{0.1}$ and (b) $CrCuFeNi_2Ti_x$ (x = 0.1, 0.3, 0.5 and 0.7) HEAs

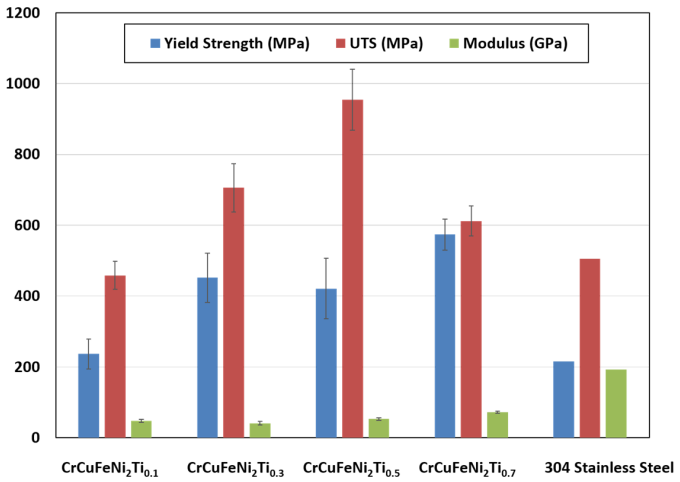

Fig. 4. Yield strength, UTS and Young's modulus of $CrCuFeNi_2Ti_x$ (x = 0.1, 0.3, 0.5 and 0.7) compared with the 304 stainless steel

Apart from dimple-like morphology, in Fig. 5 (d), the fractured surfaces exhibit some cracks, which is a significant brittle fracture behavior. And this brittle fracture behavior could possibly explain the anomalously low UTS of $CrCuFeNi_2Ti_{0.7}$ HEAs.

3.3. Hardness behavior

The hardness variation from x = 0.1 to x = 0.7 of the as-cast $CrCuFeNi_2Ti_x$ HEAs is given in Fig. 6. The hardness of the $CrCuFeNi_2Ti_{0.1}$ HEAs is about HV 151, and it increases to HV 562 as the x value changes from 0.1 to 0.7. Apparently, the hardness and strength could increase with the increasing amount of the BCC phases and the intermetallic compounds, but the alloys grow brittle in this process. More specifically, the hardness increased almost linearly from x = 0.1 to x = 0.3, where only

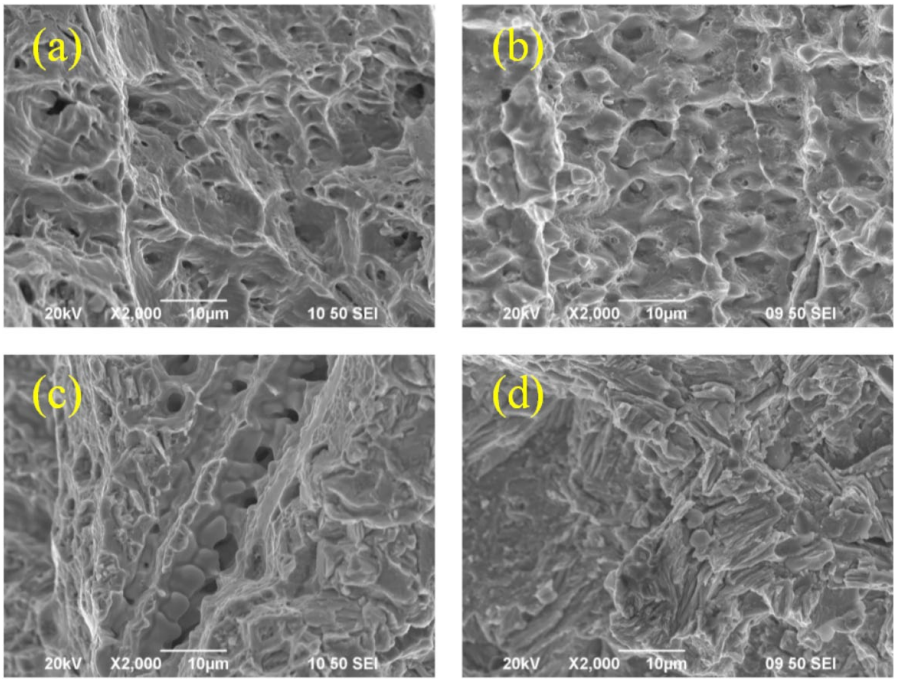

Fig. 5. Fracture surface morphology of $CrCuFeNi_2Ti_x$ (x = 0.1 (a), 0.3 (b), 0.5 (c) and 0.7 (d)

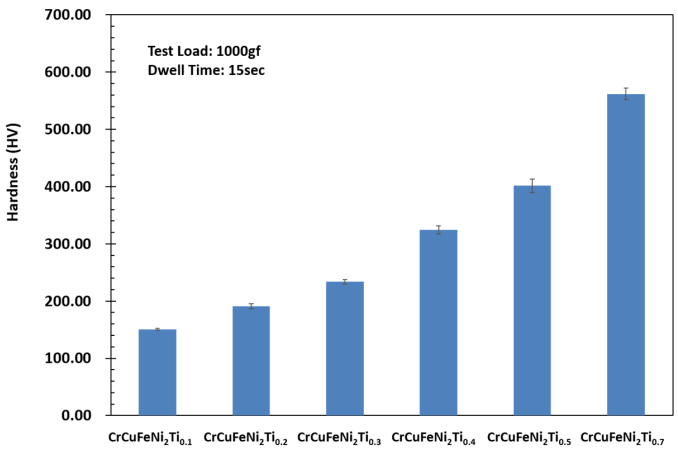

Fig. 6. Hardness for the as-cast $CrCuFeNi_2Ti_x$ (x = 0.1, 0.2, 0.3, 0.4, 0.5 and 0.7) HEAs

an FCC phase could be detected in HEAs. And the hardness increased up to HV 324 when x = 0.4, where the main phase was still FCC, but a BCC phase start to form. There was a sharp increase in hardness from HV 401 to 562 when x = 0.7. At this composition the intermetallic compounds phases have already formed.

The microstructures of the $CrCuFeNi_2Ti_x$ specimens after hardness test are shown in Fig. 7. Interestingly, slip bands around the impressions could be observed in all the specimens. Even at the stages in which the HEAs contain no BCC phase when $x \leq 0.4$. Chang et al. suggested that the occurrence of the slip bands around the indentation impression could be used to roughly gauge the plasticity of HEAs, and those showing slip bands should have good plasticity [25]. Considering that the formation of the BCC phase in HEAs tends to embrittle the material, the observed slip bands phenomena might support this argument.

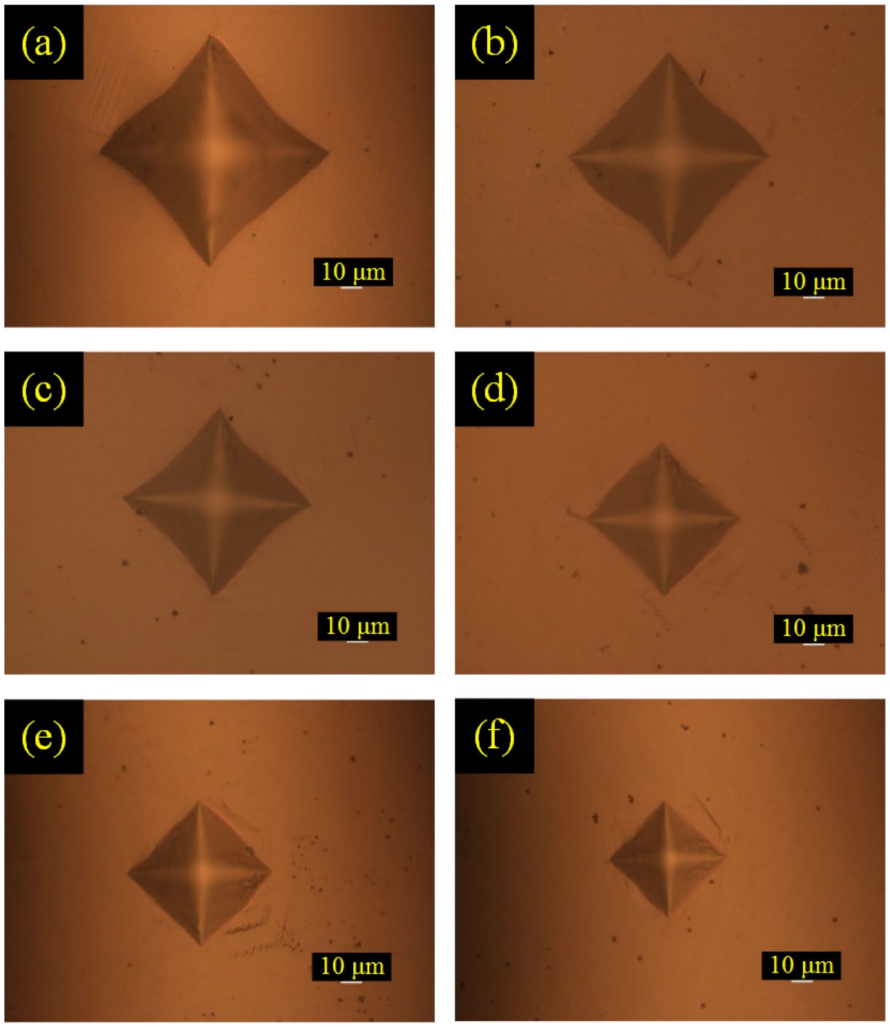

Fig. 7. Microstructures of the $CrCuFeNi_2Ti_x$ (x = 0.1 (a), 0.2 (b), 0.3 (c), 0.4 (d), 0.5 (e) and 0.7 (f) specimens after hardness test

However, the tension results indicated that the slip bands could at most be considered as an indicator of malleability (at compression), rather than ductility (at tension).

4. Conclusions

The effects of Ti content on the microstructure and tensile and hardness behaviors of $CrCuFeNi_2Ti_x$ HEAs were studied for (x = 0.1, 0.2, 0.3, 0.4, 0.5 and 0.7) in this paper. First of all, the phase selection theories, including ΔH_{mix}, ΔS_{mix}, δ, VEC, and $\Delta\chi$ values, are in accordance with the XRD patterns, which indicate that the main solid solution in $CrCuFeNi_2Ti_x$ HEAs is FCC when $x \leq 0.5$. The BCC phase and intermetallic compounds (Ni_3Ti) show up when x = 0.7. In the tensile and hardness test, the $CrCuFeNi_2Ti_x$ HEAs show low stiffness and good flexibility overall. When the x value is relatively small, the HEAs show very good ductility, and when the x value becomes larger, the HEAs show very high hardness. According to the dimple-like morphology on the fracture surface, the tensile failure of HEAs should belong to ductile fracture generally when x value is smaller than 0.5. But when x = 0.7, some crystal grains and cleavage planes can be observed on the fracture surface as well, so that both inter-granular and trans-granular brittle fracture occurs. After the hardness test, slip bands can always be found in all specimens which could be an important characteristic of the occurrence of the crystal plastic deformation.

Acknowledgments

I would like to thank Prof. Sanqiang Shi, Dr. Curtis Ng, and Mr. Zhengwen Nie in the Department of Mechanical Engineering, The Hong Kong Polytechnic University for their scientific help on this project. This work was partially supported by the Fundamental Research Funds for the Central Universities (Grant No. D5000220482) and the National Natural Science Foundation of China (NSFC) (Grant No. 62101335).

REFERENCES

[1] J.W. Yeh, S.K. Chen, S.J. Lin, J.Y. Gan, T.S. Chin, T.T. Shun, C.H. Tsau, S.Y. Chang, Nanostructured high-entropy alloys with multiple principal elements: novel alloy design concepts and outcomes, Adv. Eng. Mater. **6** (5), 299-303 (2004). DOI: https://doi.org/10.1002/adem.200300567

[2] J.-W. Yeh, S.-J. Lin, T.-S. Chin, J.-Y. Gan, S.-K. Chen, T.-T. Shun, C.-H. Tsau, S.-Y. Chou, Formation of simple crystal structures in Cu-Co-Ni-Cr-Al-Fe-Ti-V alloys with multiprincipal metallic elements, Metall. Mater. Trans. A. Phys. Metall. Mater. Sci. **35** (8), 2533-2536 (2004).

[3] C.-Y. Hsu, T.-S. Sheu, J.-W. Yeh, S.-K. Chen, Effect of iron content on wear behavior of AlCoCrFexMo$_{0.5}$Ni high-entropy alloys, Wear **268** (5-6), 653-659 (2010). DOI: https://doi.org/10.1016/j.wear.2009.10.013

[4] C.Y. Hsu, W.R. Wang, W.Y. Tang, S.K. Chen, J.W. Yeh, Microstructure and Mechanical Properties of New AlCoxCrFeMo$_{0.5}$Ni High-Entropy Alloys, Adv. Eng. Mater. **12** (1-2), 44-49 (2010). DOI: https://doi.org/10.1002/adem.200900171

[5] R. Razuan, N.A. Jani, M.K. Harun, M.K. Talari, Microstructure and Hardness Properties Investigation of Ti and Nb Added FeNiAlCuCrTi$_x$Nb$_y$ High Entropy Alloys, T. Indian. I. Metals **66** (4), 309-312 (2013). DOI: https://doi.org/10.1007/s12666-013-0265-7

[6] O. Senkov, J. Scott, S. Senkova, D. Miracle, C. Woodward, Microstructure and room temperature properties of a high-entropy TaNbHfZrTi alloy, J. Alloys. Compd. **509** (20), 6043-6048 (2011). DOI: https://doi.org/10.1016/j.jallcom.2011.02.171

[7] C.-Y. Hsu, C.-C. Juan, W.-R. Wang, T.-S. Sheu, J.-W. Yeh, S.-K. Chen, On the superior hot hardness and softening resistance of AlCoCrxFeMo$_{0.5}$Ni high-entropy alloys, Metall. Mater. Trans. A. Phys. Metall. Mater. Sci. **528** (10-11), 3581-3588 (2011). DOI: https://doi.org/10.1016/j.msea.2011.01.072

[8] Y. Zhou, Y. Zhang, Y. Wang, G. Chen, Solid solution alloys of AlCoCrFeNiTi$_x$ with excellent room-temperature mechanical properties. Appl. Phys. Lett. **90** (18), 181904 (2007). DOI: https://doi.org/10.1063/1.2734517

[9] O. Senkov, J. Scott, S. Senkova, F. Meisenkothen, D. Miracle, C. Woodward, Microstructure and elevated temperature properties of a refractory TaNbHfZrTi alloy, J. Mater. Sci. **47** (9), 4062-4074 (2012). DOI: https://doi.org/10.1007/s10853-012-6260-2

[10] R.A. Sekhar, N. Nayan, S.R. Bakshi, Microstructure and Mechanical Properties of NiTiCuFe Multi-component Alloy, T. Indian. I. Metals **71** (11), 2789-2793 (2018). DOI: https://doi.org/10.1007/s12666-018-1444-3

[11] R.A. Sekhar, S.R. Bakshi, Microstructure and Mechanical Properties of Ti–Al–Ni–Cr–Co–Fe-Based High-Entropy Alloys. T. Indian. I. Metals **72** (6), 1413-1416 (2019). DOI: https://doi.org/10.1007/s12666-019-01708-x

[12] M.-H. Chuang, M.-H. Tsai, W.-R. Wang, S.-J. Lin, J.-W. Yeh, Microstructure and wear behavior of AlxCo$_{1.5}$CrFeNi$_{1.5}$Ti$_y$ high-entropy alloys, Acta. Mater. **59** (16), 6308-6317 (2011). DOI: https://doi.org/10.1016/j.actamat.2011.06.041

[13] C. Li, J. Li, M. Zhao, Q. Jiang, Effect of alloying elements on microstructure and properties of multiprincipal elements high-entropy alloys, J. Alloys. Compd. **475** (1-2), 752-757 (2009). DOI: https://doi.org/10.1016/j.jallcom.2008.07.124

[14] B.S. Murty, J.-W. Yeh, S. Ranganathan, P. Bhattacharjee, High-entropy alloys, 2019 Elsevier.

[15] S. Ranganathan, Alloyed pleasures: multimetallic cocktails, Curr. Sci. India. **85** (10), 1404-1406 (2003).

[16] Y. Zhang, Y.J. Zhou, Solid solution formation criteria for high entropy alloys, Mater. Sci. Forum. **561-565**, 1337-1339 (2007). DOI: https://doi.org/10.4028/www.scientific.net/MSF.561-565.1337

[17] Y. Zhang, Y.J. Zhou, J.P. Lin, G.L. Chen, P.K. Liaw, Solid-solution phase formation rules for multi-component alloys, Adv. Eng. Mater. **10** (6), 534-538 (2008). DOI: https://doi.org/10.1002/adem.200700240

[18] S. Guo, C. Ng, J. Lu, C. Liu, Effect of valence electron concentration on stability of fcc or bcc phase in high entropy alloys, J. Appl. Phys. **109** (10), 103505 (2011). DOI: https://doi.org/10.1063/1.3587228

[19] S. Guo, C.T. Liu, Phase stability in high entropy alloys: formation of solid-solution phase or amorphous phase, Prog. Nat. Sci-mater. **21** (6), 433-446 (2011). DOI: https://doi.org/10.1016/S1002-0071(12)60080-X

[20] S. Fang, Z. Zhou, J. Zhang, M. Yao, F. Feng, D. Northwood, Two mathematical models for the hydrogen storage properties of AB2 type alloys, J. Alloys. Compd. **293-295**, 10-13 (1999). DOI: https://doi.org/10.1016/S0925-8388(99)00380-1

[21] C. Ng, S. Guo, J. Luan, S. Shi, C.T. Liu, Entropy-driven phase stability and slow diffusion kinetics in an Al$_{0.5}$CoCrCuFeNi high entropy alloy, Intermetallics **31**, 165-172 (2012). DOI: https://doi.org/10.1016/j.intermet.2012.07.001

[22] C. Ng, S. Guo, J. Luan, Q. Wang, J. Lu, S. Shi, C.T. Liu, Phase stability and tensile properties of Co-free Al$_{0.5}$CrCuFeNi$_2$ high-entropy alloys, J. Alloys. Compd. **584**, 530-537 (2014). DOI: https://doi.org/10.1016/j.jallcom.2013.09.105

[23] Y. Zhang, G. Chen, C. Gan, Phase Change and Mechanical Behaviors of Ti$_x$CoCrFeNiCu$_{1-y}$Al$_y$ High Entropy Alloys, J. ASTM. Int. **7** (5), 1-8 (2010). DOI: https://doi.org/10.1520/JAI102527

[24] C. Ng, S. Guo, J. Luan, Q. Wang, J. Lu, S. Shi, C. Liu, Phase stability and tensile properties of Co-free Al$_{0.5}$CrCuFeNi$_2$ high-entropy alloys, J. Alloys. Compd. **584**, 530-537 (2014). DOI: https://doi.org/10.1016/j.jallcom.2013.09.105

[25] C. Chang, Microstructure and Properties of As-Cast 10-Component Nanostructured AlCoCrCuFeMoNiTiVZr High-Entropy Alloy, PhD thesis, National Tsing Hua University, 2004.

[26] A. Takeuchi, A. Inoue, Classification of bulk metallic glasses by atomic size difference, heat of mixing and period of constituent elements and its application to characterization of the main alloying element, Mater. Trans. **46** (12), 2817-2829 (2005). DOI: https://doi.org/10.2320/matertrans.46.2817

[27] L. Han, Y.B. Wang, Y. Zhang, C. Lu, C.W. Fei, Y.J. Zhao, Competitive cracking behavior and microscopic mechanism of Ni-based superalloy blade respecting accelerated CCF failure, Int. J. Fatigue. **150**, 106306 (2021). DOI: https://doi.org/10.1016/j.ijfatigue.2021.106306

[28] J. Yeh, Recent progress in high-entropy alloys, Ann. Chimie. Sci. Materiaux. **31** (6), 633-648 (2006). DOI: https://doi.org/10.3166/acsm.31.633-648

[29] C. Lu, C.W. Fei, Y.W. Feng, Y.J. Zhao, X.W. Dong, Probabilistic analyses of structural dynamic response with modified Kriging-based moving extremum framework, Eng. Fail. Anal. 1**25**, 105398 (2021). DOI: https://doi.org/10.1016/j.engfailanal.2021.105398